

1 **Increased Potency and Breadth of SARS-CoV-2 Neutralizing Antibodies After a Third**
2 **mRNA Vaccine Dose**

3
4 Frauke Muecksch^{1,*}, Zijun Wang^{2,*}, Alice Cho^{2,*}, Christian Gaebler², Tarek Ben Tanfous², Justin
5 DaSilva¹, Eva Bednarski¹, Victor Ramos², Shuai Zong², Brianna Johnson², Raphael Raspe²,
6 Dennis Schaefer-Babajew², Irina Shimeliovich², Mridushi Daga², Kai-Hui Yao², Fabian
7 Schmidt¹, Katrina G. Millard², Martina Turroja², Mila Jankovic², Thiago Y. Oliveria², Anna
8 Gazumyan², Marina Caskey², Theodora Hatzioannou¹, Paul D. Bieniasz^{1,3}, and Michel C.
9 Nussenzweig^{2,3}.

10
11 ¹Laboratory of Retrovirology, The Rockefeller University, New York, NY 10065, USA

12 ²Laboratory of Molecular Immunology, The Rockefeller University, New York, NY 10065, USA

13 ³Howard Hughes Medical Institute

14
15 *equal contribution

16 Address correspondence to: Theodora Hatzioannou thatziio@rockefeller.edu; Paul D. Bieniasz
17 pbieniasz@rockefeller.edu; or Michel C. Nussenzweig nussen@rockefeller.edu
18
19
20
21

22 **Abstract**

23 **The omicron variant of SARS-CoV-2 infected very large numbers of SARS-CoV-2**
24 **vaccinated and convalescent individuals¹⁻³. The penetrance of this variant in the antigen**
25 **experienced human population can be explained in part by the relatively low levels of plasma**
26 **neutralizing activity against Omicron in people who were infected or vaccinated with the**
27 **original Wuhan-Hu-1 strain⁴⁻⁷. The 3rd mRNA vaccine dose produces an initial increase in**
28 **circulating anti-Omicron neutralizing antibodies, but titers remain 10-20-fold lower than**
29 **against Wuhan-Hu-1 and are, in many cases, insufficient to prevent infection⁷. Despite the**
30 **reduced protection from infection, individuals that received 3 doses of an mRNA vaccine**
31 **were highly protected from the more serious consequences of infection⁸. Here we examine**
32 **the memory B cell repertoire in a longitudinal cohort of individuals receiving 3 mRNA**
33 **vaccine doses^{9,10}. We find that the 3rd dose is accompanied by an increase in, and evolution**
34 **of, anti-receptor binding domain specific memory B cells. The increase is due to expansion**
35 **of memory B cell clones that were present after the 2nd vaccine dose as well as the emergence**
36 **of new clones. The antibodies encoded by these cells showed significantly increased potency**
37 **and breadth when compared to antibodies obtained after the 2nd vaccine dose. Notably, the**
38 **increase in potency was especially evident among newly developing clones of memory cells**
39 **that differed from the persisting clones in targeting more conserved regions of the RBD.**
40 **Overall, more than 50% of the analyzed neutralizing antibodies in the memory compartment**
41 **obtained from individuals receiving a 3rd mRNA vaccine dose neutralized Omicron. Thus,**
42 **individuals receiving 3 doses of an mRNA vaccine encoding Wuhan-Hu-1, have a diverse**
43 **memory B cell repertoire that can respond rapidly and produce antibodies capable of**
44 **clearing even diversified variants such as Omicron. These data help explain why a 3rd dose**
45 **of an mRNA vaccine that was not specifically designed to protect against variants is effective**
46 **against variant-induced serious disease.**

47

48

49 **Main**

50 We studied the immune responses to SARS-CoV-2 mRNA vaccination in a longitudinal cohort of
51 43 volunteers with no prior history of SARS-CoV-2 infection^{9,10}, who were recruited between
52 January 21, 2021, and December 14, 2021, for sequential blood donation. Volunteers received
53 either the Moderna (mRNA-1273; n=8) or Pfizer-BioNTech (BNT162b2; n=35) mRNA vaccines.
54 The volunteers ranged in age from 23-78 years old 53% were male and 47% female (for details
55 see Methods and Supplementary Table 1). Samples were obtained at the following time points: 1)
56 2.5 weeks after the prime; 2) 1.3 and 5 months after the 2nd vaccine dose; 3) 1 month after the 3rd
57 dose.

58

59 **Plasma binding and neutralization**

60 Plasma IgM, IgG and IgA responses to SARS-CoV-2 RBD were measured by enzyme-linked
61 immunosorbent assay (ELISA)^{9,10}. After a significant decrease in antibody reactivity during the 5
62 months following the second vaccine dose, anti-RBD IgG titers were significantly increased
63 following a 3rd dose of an mRNA vaccine ($p < 0.0001$, Fig. 1a and Supplementary Table 1). The
64 resulting titers were similar to those found 1.3 months after the 2nd dose ($p > 0.99$, Fig. 1a). IgM
65 and IgA titers were lower than IgG titers and while IgM titers were unchanged during the
66 observation period, IgA titers also increased significantly following a 3rd vaccine dose (Extended
67 data Fig. 1 and Supplementary Table 1).

68

69 Plasma neutralizing activity in 43 participants was measured using HIV-1 pseudotyped with the
70 Wuhan-Hu-1 SARS-CoV-2 spike protein^{9,10} (Fig. 1b and Supplementary Table 1). Following a
71 7.4-fold decrease in neutralizing titers between 1.3- and 5-months after the 2nd vaccine dose,
72 administration of a 3rd vaccine dose boosted neutralizing titers 11.8-fold resulting in a geometric
73 mean half-maximal neutralizing titer (NT₅₀) of 3,199 against Wuhan-Hu-1 (Fig. 1b). Plasma
74 neutralizing antibodies elicited by mRNA vaccination are more potent against Wuhan-Hu-1 than
75 variants^{9,10}. Consistent with prior reports^{3,7,11-13}, the 3rd vaccine dose significantly boosts geometric
76 mean NT₅₀s 16-fold, 12-fold and 37-fold for the Beta, Delta and Omicron variant, respectively.
77 The level of activity against the Beta and Delta variants was not significantly different than against
78 Wuhan-Hu-1 while the activity against Omicron was 16-fold lower than against Wuhan-Hu-1
79 ($p = 0.58$, $p = 0.24$ and $p = 0.0013$, respectively. Fig. 1c). Given the correlation between neutralizing

80 antibody levels and protection from infection^{14,15}, the reduced activity against Omicron in 3rd dose
81 vaccine recipients is likely to explain why vaccinees remain particularly susceptible to infection
82 by this variant.

83

84 **Memory B cells**

85 Under physiologic conditions memory B cells produce little if any secreted antibody. However,
86 when challenged with antigen as in a breakthrough infection, these cells undergo clonal expansion
87 and produce antibody secreting plasma cells, memory and germinal center B cells¹⁶. To examine
88 the effects of the 3rd vaccine dose on the memory compartment in our longitudinal cohort we
89 performed flow cytometry experiments using phycoerythrin (PE) and Alexa Fluor 647 (AF647)
90 labeled RBDs (Fig. 2a and Extended data Fig. 2). Individuals that received a 3rd vaccine dose
91 developed significantly increased numbers of RBD-binding memory cells compared to the 2nd dose
92 or naturally infected individuals^{9,10,17} (Fig. 2a and b). The number of memory cells produced after
93 the 3rd dose was also higher than for vaccinated convalescent individuals but did not reach
94 significance ($p=0.08$, Fig 2b). An increased proportion of memory B cells circulating after the 3rd
95 dose expressed IgG and lower levels of CD71 suggesting that germinal center-derived memory B
96 cells dominate this compartment (Extended data Fig. 2c).

97

98 We obtained 1370 paired antibody sequences from 5 individuals who were sampled 5 months after
99 the 2nd and 1 month after the 3rd vaccine dose. Two and 3 out of those participants were additionally
100 sampled 2.5 weeks after the first dose and 1.3 months after the second dose, respectively (^{9,10}, Fig.
101 2c, Supplementary Table 2). After the 3rd vaccine dose all individuals examined showed expanded
102 clones of memory B cells (Fig. 2c). Like earlier time points there was over-representation of VH3-
103 30, VH3-53 and VH4-31 genes (^{9,10} and Extended data Fig. 3). Thus, there is a persistent bias in
104 IGVH gene representation in memory which is common to most individuals.

105

106 Expanded clones of memory cells accounted for 33% and 47% of the repertoire 5 months after the
107 2nd and 1 month after the 3rd dose, respectively (Fig. 2c and Extended data Fig. 4a). The relative
108 increase in clonality was due in part to an average 3.1-fold expansion of persisting anti-RBD-
109 specific memory B cells ($p<0.0001$, Fig. 2d). Consistent with the relatively modest number of
110 additional cell divisions by persisting clones, they accumulated on average only 2 additional

111 somatic hypermutations making it unlikely that the additional clonal expansion required further
112 germinal center residence¹⁶ (Fig. 2e and Extended data Fig. 4b).

113

114 There was also a more modest 1.7-fold increase in the number of newly emerging unique clones
115 of memory cells after the 3rd dose that did not reach statistical significance ($p=0.09$) (Fig. 2d).
116 These cells were more mutated than the unique clones present 5 months after the 2nd vaccine dose
117 as were antibodies that were represented only once (singlets). In both cases the numbers of somatic
118 mutations were significantly greater than at 5 months after the 2nd dose indicating persisting
119 evolution and cell division ($p=0.0009$ and $p<0.0001$, respectively. Fig. 2e and Extended data Fig.
120 4). In conclusion, the 3rd mRNA vaccine dose is associated with expansion and further evolution
121 of the memory B cell compartment.

122

123 **Monoclonal antibodies**

124 472 monoclonal antibodies obtained from different time points were expressed and tested by
125 ELISA, 459 bound to Wuhan-Hu-1 RBD indicating the high efficiency of the RBD-specific
126 memory B cell isolation method employed here (Extended data Fig. 5 and Supplementary Table
127 3). 191 antibodies obtained after the 3rd vaccine dose were compared to 34 isolated after the prime;
128 79 and 168 isolated 1.3 and 5 months after the 2nd vaccine dose (Vax2-1.3m and Vax2-5m),
129 respectively. The geometric mean ELISA half-maximal concentration (EC_{50}) of the RBD-binding
130 antibodies was 4.4, 3.8, 2.9 and 3.5 ng/ml for antibodies isolated at the prime, Vax2-1.3-months,
131 Vax2-5-months and Vax3-1-month timepoints, respectively (Extended data Fig. 5a and
132 Supplementary Table 3). Overall, there was no significant change in binding over time or the
133 number of vaccine doses. This was true for all antibodies combined, as well as for persisting
134 clones, unique clones that could only be detected at a single timepoint, and single antibodies
135 (Extended data Fig. 5a-c).

136

137 All 459 RBD-binding antibodies were subjected to a SARS-CoV-2 pseudotype neutralization
138 assay based on the Wuhan-Hu-1 SARS-CoV-2 spike^{9,10}. Between 1.3- and 5-months after the 2nd
139 vaccine dose antibody potency improved but did not reach statistical significance (IC_{50} 290 vs.
140 182, $p=0.60$ Fig 3a). There was additional improvement after the 3rd vaccine dose (IC_{50} 182 vs.
141 111, $p=0.049$ Fig. 3a). The overall improvement between equivalent time points after the 2nd and

142 the 3rd dose, from IC₅₀ 290 ng/ml to 111 ng/ml was highly significant (p=0.0023, Fig. 3a and
143 Supplementary Table 3). Notably, the potency of antibodies isolated after the 3rd dose,
144 approximately 10 months (293 (223-448) days) after the prime-dose, was indistinguishable from
145 antibodies isolated from convalescent vaccinated individuals 12 months after infection (p=0.69,
146 Fig. 3a) ¹⁷⁻¹⁹. The improved neutralizing activity was most evident among unique clones with a
147 dramatic change in IC₅₀ from 323 to 67ng/ml, p=0.034 (Fig. 3b and Supplementary Table 3).
148 Persisting clones also showed improved neutralizing activity after the 3rd dose (p=0.043, Fig. 3b)
149 and a trend to improved neutralizing activity was evident among single antibodies but this did not
150 reach statistical significance (Fig. 3b, Extended data Fig. 5d and Supplementary Table 3 and 4). In
151 all cases, the relative potency of the antibodies isolated 1 month after the 3rd dose was similar to
152 the antibodies isolated from convalescent vaccinated individuals 12 months after infection (Fig.
153 3a and b). Taken together, there is a significant improvement in the neutralizing potency of the
154 antibodies expressed in the memory B cell compartment 1 month after administration of the 3rd
155 mRNA vaccine dose compared to 1.3 months after the 2nd dose. Newly detected singlets and clones
156 of expanded memory B cells account for most of the improvement in neutralizing activity between
157 5 months after 2nd dose and 1 month after the 3rd dose.

158

159 **Epitopes and Neutralization Breadth**

160 The majority of the anti-RBD neutralizing antibodies obtained from vaccinated individuals after
161 the 2nd vaccine dose belong to class 1 and 2 that target a region overlapping with the ACE2 binding
162 site ^{20,21} (Fig. 4a). These antibodies are generally more potent than class 3 and 4 antibodies that
163 target the more conserved base of the RBD and do not directly interfere with ACE2 binding (¹⁷,
164 Fig. 4a and Extended data Fig. 6). Whereas class 1 and 2 antibodies that develop early are
165 susceptible to mutations in and around the ACE2 binding site found in many of the variants of
166 concern, evolved versions of the same antibodies can be resistant^{17,22}. Based on structural
167 information and sequence conservation among betacoronaviruses, antibodies that span class 3 or
168 4 and either class 1 or 2 could be broadly active (Fig. 4b and Extended data Fig. 6).

169

170 To examine epitopes targeted by RBD-binding antibodies after the 3rd vaccine dose, we performed
171 BLI experiments in which a preformed antibody-RBD complex was exposed to a second antibody
172 targeting one of four classes of structurally defined epitopes (C105 as Class 1; C144 as Class 2,

173 C135 as Class 3 and C118 as Class 1/4^{18,20}) (Fig. 4a). 168 random RBD binding antibodies were
174 tested among which 20, 29, and 36 neutralized with IC₅₀s lower than 1000 ng/ml from 1.3 and 5-
175 months after the 2nd and 1 month after the 3rd vaccine dose respectively. As might be expected the
176 largest group of RBD binding antibodies obtained after the 2nd vaccine dose belonged to class 1/2
177 (Fig. 4c). Although the overall distribution of antibody classes that bind to RBD did not change
178 significantly between 1.3 and 5-months after the 2nd dose, the relative representation of class 1 and
179 2 antibodies decreased (Fig. 4c). This trend continued after the 3rd vaccine dose with increased
180 representation of RBD binding antibodies in class 1/4 and 3 resulting in a significant difference in
181 the epitope distribution among RBD-binding antibodies between the early time points after the 2nd
182 and the 3rd dose (p=0.005, Fig. 4c). As expected, these differences can be accounted for primarily
183 by the emergence of new clones and singlets after the 3rd vaccine dose (Fig. 4d). Similar results
184 were found when considering the neutralizing antibodies with initial dominance of class 1/2 and
185 increasing representation of class 1/4 and 3 over time (Fig. 4e).

186

187 The neutralizing breadth of antibodies elicited by infection increased significantly after 5 months
188 ^{17,19,22}. There was also a trend to increased breadth that did not reach statistical significance 5
189 months after the 2nd dose of an mRNA vaccine¹⁰. To determine whether neutralizing antibodies in
190 clones that persisted from 5 months after the 2nd to 1 month after the 3rd dose develop increased
191 breadth, we compared 18 antibody pairs. Neutralizing activity was measured against a panel of
192 SARS-CoV-2 pseudoviruses harboring RBD amino acid substitutions representative of SARS-
193 CoV-2 variants including Delta and Omicron (Fig. 5a). The clonal pairs were dominated by
194 antibodies belonging to class 1/2, 2/3 and 3, as determined by BLI (Fig 5a). 15 out of 18 antibody
195 pairs neutralized the pseudovirus carrying the Delta RBD-amino acid substitutions at low antibody
196 concentrations at both time points, with IC₅₀ values ranging from 1-154 ng/ml (Fig. 5a). While the
197 Omicron pseudovirus showed the highest degree of neutralization resistance, 11 out of 18
198 antibodies isolated 1 month after the 3rd dose neutralized this virus, 9 of those at IC₅₀s below 120
199 ng/ml (Fig. 5a). Most antibody pairs isolated before and after the 3rd vaccine dose showed
200 exceptionally broad neutralization and there was little change in antibody breadth within the
201 analyzed pairs (Fig. 5a).

202

203 We extended the analysis to compare the activity of antibodies present in memory cells found 1.3
204 months after the 2nd and unique to 1 month after the 3rd vaccine dose. The antibodies were tested
205 against viruses pseudotyped with spike proteins containing the RBD of Wuhan-Hu-1, Delta and
206 Omicron (Fig. 5b). We found that the proportion of Omicron-neutralizing antibodies increased
207 from 15% after the 2nd dose to 50% among the unique antibodies found after the 3rd dose ($p=0.035$,
208 Fisher's exact test. Fig 5b). Among all antibodies evaluated, the increase in breadth between the
209 2nd and 3rd vaccine dose was reflected by an increase in potency from 689 to 124 ng/ml IC₅₀ against
210 Omicron ($p=0.0004$, Fig 5c). Similar results were seen for Delta neutralization (Fig. 5c). Thus,
211 memory B cell clones emerging after the 3rd vaccine dose show increasing breadth and potency
212 against pseudoviruses representing variants that were not present in the vaccine.

213
214 Finally, we compared the neutralization breadth of 3rd dose vaccine-elicited antibodies, as
215 measured approximately 10 months (292 (223-448) days) after the prime dose, with antibodies we
216 obtained from a cohort of convalescent unvaccinated individuals 12 months after infection (¹⁷⁻¹⁹
217 and Fig. 5d). The two groups of antibodies are equally and remarkably broad. 92% and 94% of the
218 convalescent and 3rd dose antibodies neutralized pseudoviruses carrying the Beta-RBD and 27%
219 and 56%, respectively, neutralized Omicron. Thus, 3rd dose vaccine-elicited antibodies are at least
220 as broad as those elicited by infection (Fig. 5d).

221

222 **Discussion**

223 Memory B cells can develop from the germinal center or directly from a germinal center
224 independent activated B cell compartment¹⁶. B cells residing in germinal centers undergo multiple
225 rounds of division, mutation and selection, whereas those in the activated compartment undergo
226 only a limited number of divisions and carry fewer mutations¹⁶. Both pathways remain active
227 throughout the immune response^{23,24}. Our data indicate that the 3rd dose of mRNA vaccines against
228 SARS-CoV-2 expands persisting clones of memory B cells through the germinal center
229 independent compartment because these cells show limited clonal expansion and accumulate a
230 small number of additional mutations. In addition, however, the 3rd dose elicits a cohort of
231 previously undetected clones that carry mutations indicative of germinal center residence. The
232 later differ from the persistent clones in that they appear to target more conserved regions of the
233 RBD. Several different mechanisms could account for the antigenic shift including epitope

234 masking by the high affinity antibodies elicited by earlier vaccine doses that primarily target the
235 less conserved receptor binding domain of the RBD^{20,21,25}.

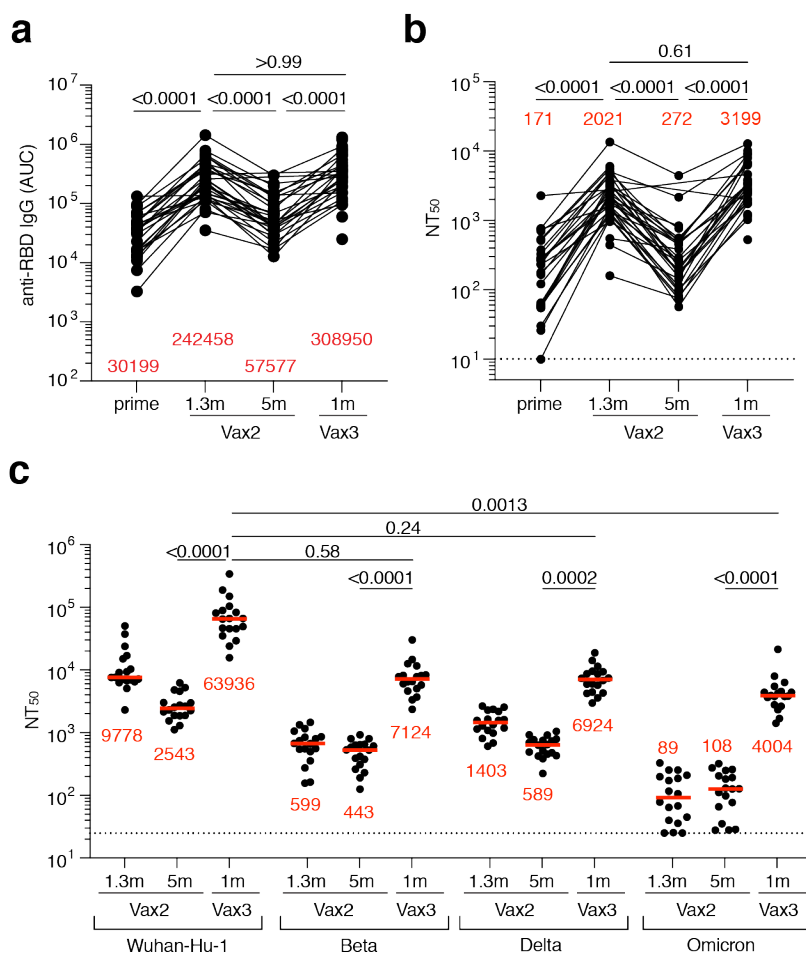
236

237 Passively administered antibodies are protective against SARS-CoV-2 infection and can also
238 prevent serious disease if provided early²⁶⁻³⁰. The 3rd dose of mRNA vaccines boosts plasma
239 antibody responses to multiple SARS-CoV-2 variants including Omicron, but the levels are
240 insufficient to prevent breakthrough infection in many individuals^{2,3}. The 3rd dose also elicits
241 increased number of memory B cells that express more potent and broader antibodies. These cells
242 do not appear to contribute to circulating plasma antibody levels, but upon challenge with antigen
243 in the form of a vaccine or infection, they produce large amounts of antibodies within 3-5 days³¹.
244 Passive administration of antibodies within this same time window prevents the most serious
245 consequences of infection^{26,29,32}. Thus, rapid recall by a diversified and expanded memory B cell
246 compartment is likely to be one of the key mechanisms that contribute to the enhanced protection
247 against severe disease by a 3rd mRNA vaccine dose.

248

249

250 **Main figures**



251

252 **Fig. 1: Plasma ELISAs and neutralizing activity.**

253 **a**, Graph shows area under the curve (AUC) for plasma IgG antibody binding to SARS-CoV-2

254 RBD after prime¹⁰, 1.3 months (m) and 5 months (m) post-second vaccination (Vax2)^{9,10}, and 1

255 month after third vaccination booster (Vax3) for n=43 samples. Lines connect longitudinal

256 samples. **b**, Graph shows anti-SARS-CoV-2 NT₅₀s of plasma measured by a SARS-CoV-2

257 pseudotype virus neutralization assay using wild-type (Wuhan Hu-1³³) SARS-CoV-2

258 pseudovirus^{18,34} in plasma samples shown in panel **a**. **c**, Plasma neutralizing activity against

259 indicated SARS-CoV-2 variants of interest/concern for n=15 randomly selected samples. Wuhan-

260 Hu-1 and Omicron NT₅₀ values are derived from ⁷. See Methods for a list of all

261 substitutions/deletions/insertions in the spike variants. All experiments were performed at least in

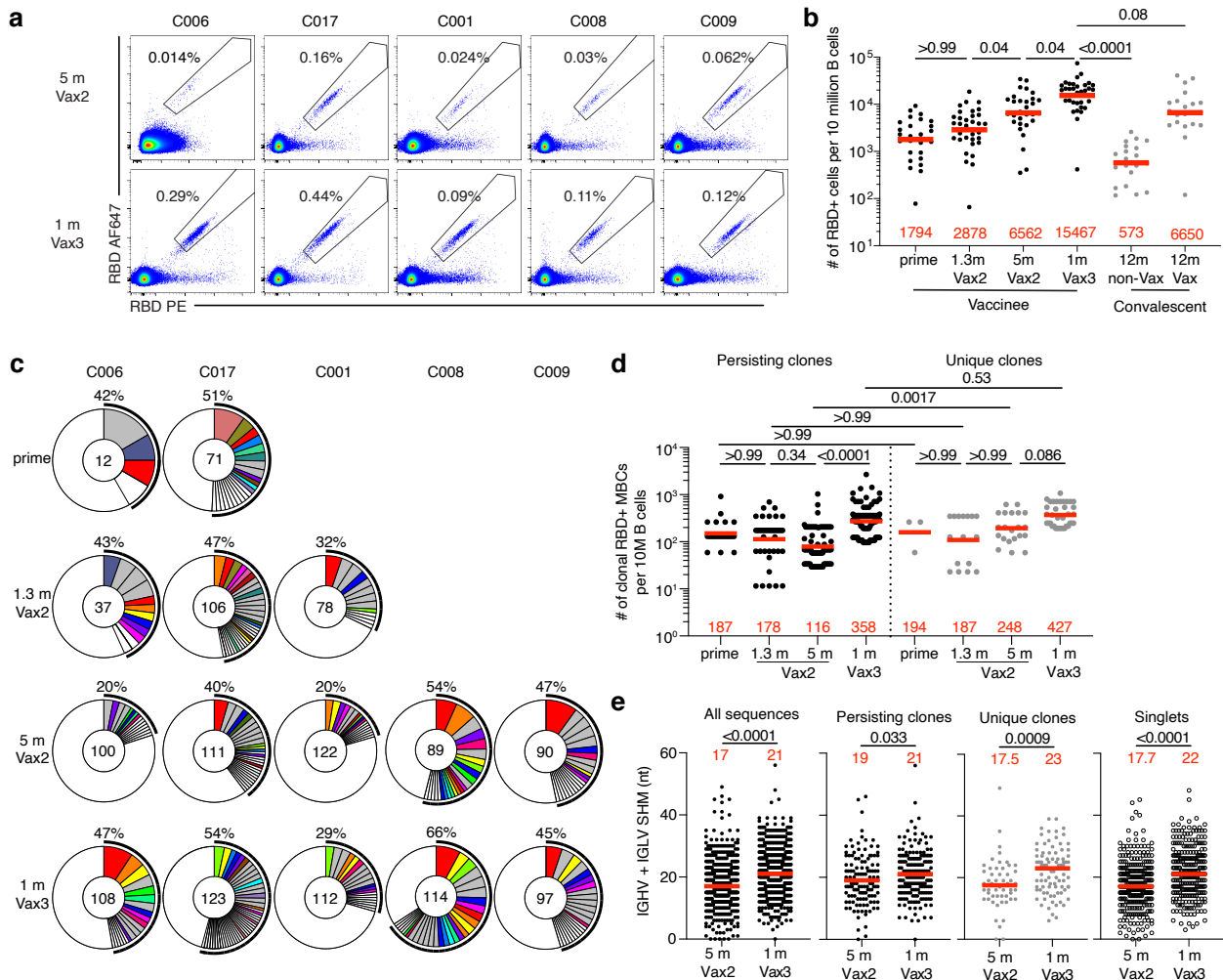
262 duplicate. Red bars and values in **a**, **b**, and **c** represent geometric mean values. Statistical

263 significance in **a-b** was determined by two-tailed Kruskal-Wallis test with subsequent Dunn's

264 multiple comparisons. Statistical significance in **c** was determined by Friedman-test with

265 subsequent Dunn's multiple comparisons.

266



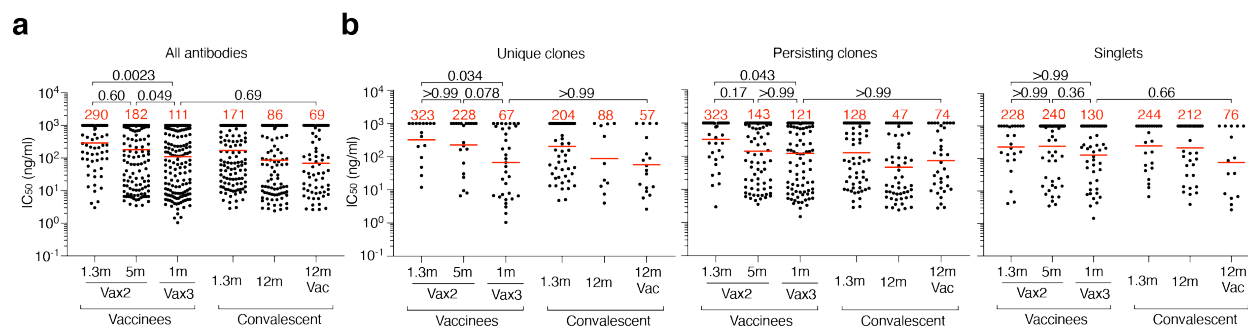
267

268 **Fig. 2: Anti-SARS-CoV-2 RBD memory B cells after third vaccination.** **a**, Representative flow
 269 cytometry plots showing dual AlexaFluor-647-RBD and PE-RBD-binding, single-cell sorted B
 270 cells from 5 individuals 5 months after Vax2¹⁰ and 1 month after the 3rd vaccine dose (Vax3).
 271 Gating strategy is shown in Extended Data Fig. 2. Percentage of RBD-specific B cells is indicated.
 272 **b**, Graph summarizing the number of Wuhan-Hu-1 RBD-specific memory B cells (MBCs) per 10
 273 million B cells after prime^{9,10}, 1.3- and 5-months after Vax2^{9,10}, and 1 month after the 3rd vaccine
 274 dose (n=43), compared to the number of RBD-specific MBCs detected in convalescent infected
 275 individuals 12-months after infection with or without later vaccination¹⁷ (shown here in grey). **c**,
 276 Pie charts show the distribution of IgG antibody sequences obtained from memory B cells from 5
 277 individuals after prime¹⁰, 1.3-months and 5-months post-Vax2^{9,10}, and 1 month after the 3rd
 278 vaccine dose. Time points indicated to the left of the charts. The number inside the circle indicates
 279 the number of sequences analyzed for the individual denoted above the circle. Pie slice size is
 280 proportional to the number of clonally related sequences. The black outline and associated
 281 numbers indicate the percentage of clonal sequences detected at each time point. Colored slices
 282 indicate persisting clones (same *IGHV* and *IGLV* genes, with highly similar CDR3s) found at more
 283 than one timepoint within the same individual. Grey slices indicate clones unique to the timepoint.
 284 White slices indicate repeating sequences isolated only once per time point. **d**, Graph shows the

285 number of clonal RBD-specific MBCs per 10 million B cells. Each dot represents one clone
 286 illustrated in Fig. 2c. Left panel (black dots) represent persisting clones. Right panel (grey dots)
 287 represent time point unique clones. **e**, Number of nucleotide somatic hypermutations (SHM) in
 288 *IGHV* + *IGLV* in all sequences detected 5 months after Vax2¹⁰ or 1 month after Vax3, compared
 289 to SHM in *IGHV* + *IGLV* of sequences from persisting clones, unique clones, and singlets. Red
 290 bars and numbers in **b**, and **d**, represent geometric mean value at each time point, and in **e**, represent
 291 median values. Statistic difference in **b**, and **d**, was determined by determined by two-tailed
 292 Kruskal Wallis test with subsequent Dunn's multiple comparisons, and in **e**, by two-tailed Mann-
 293 Whitney test.

294

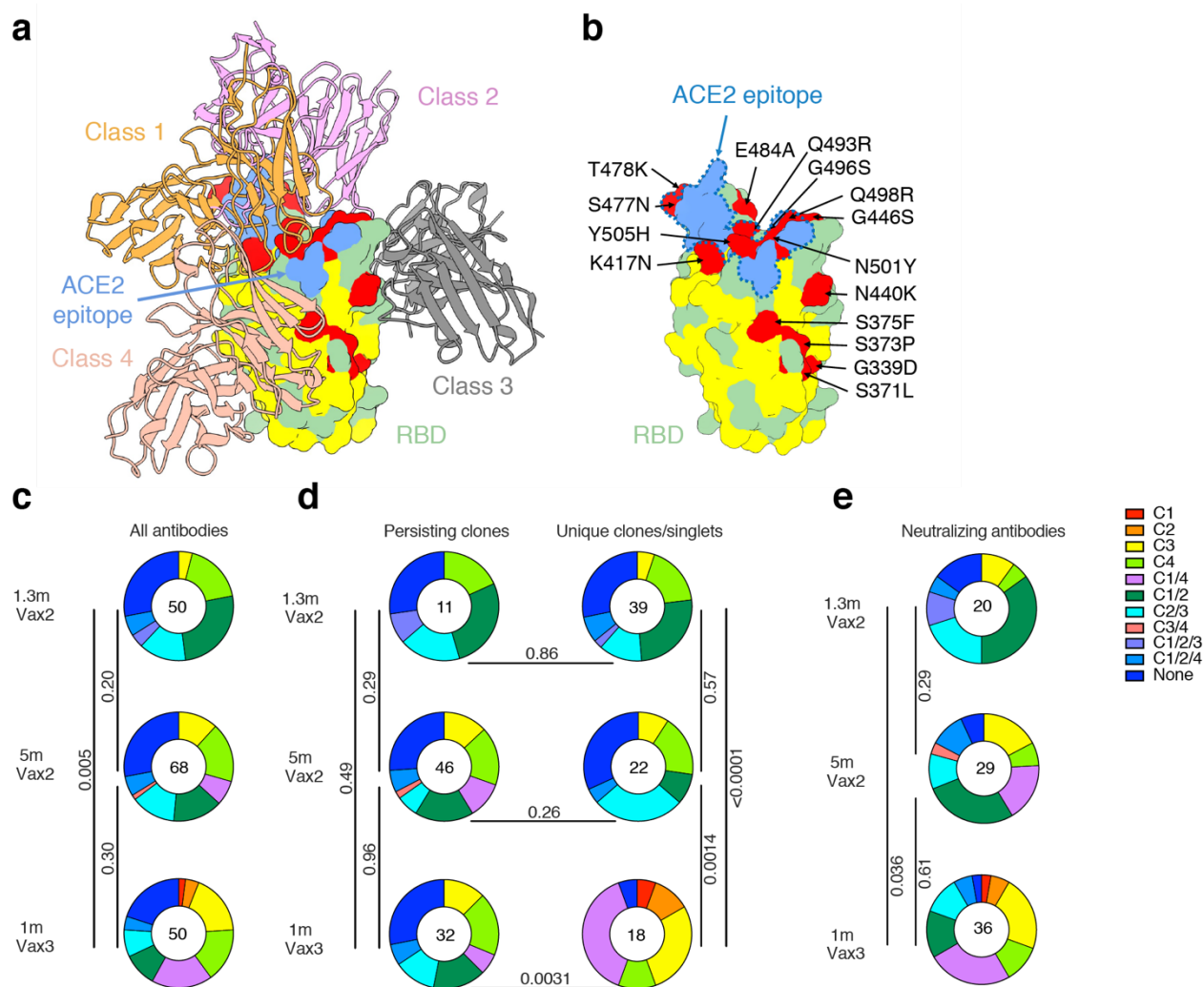
295



296

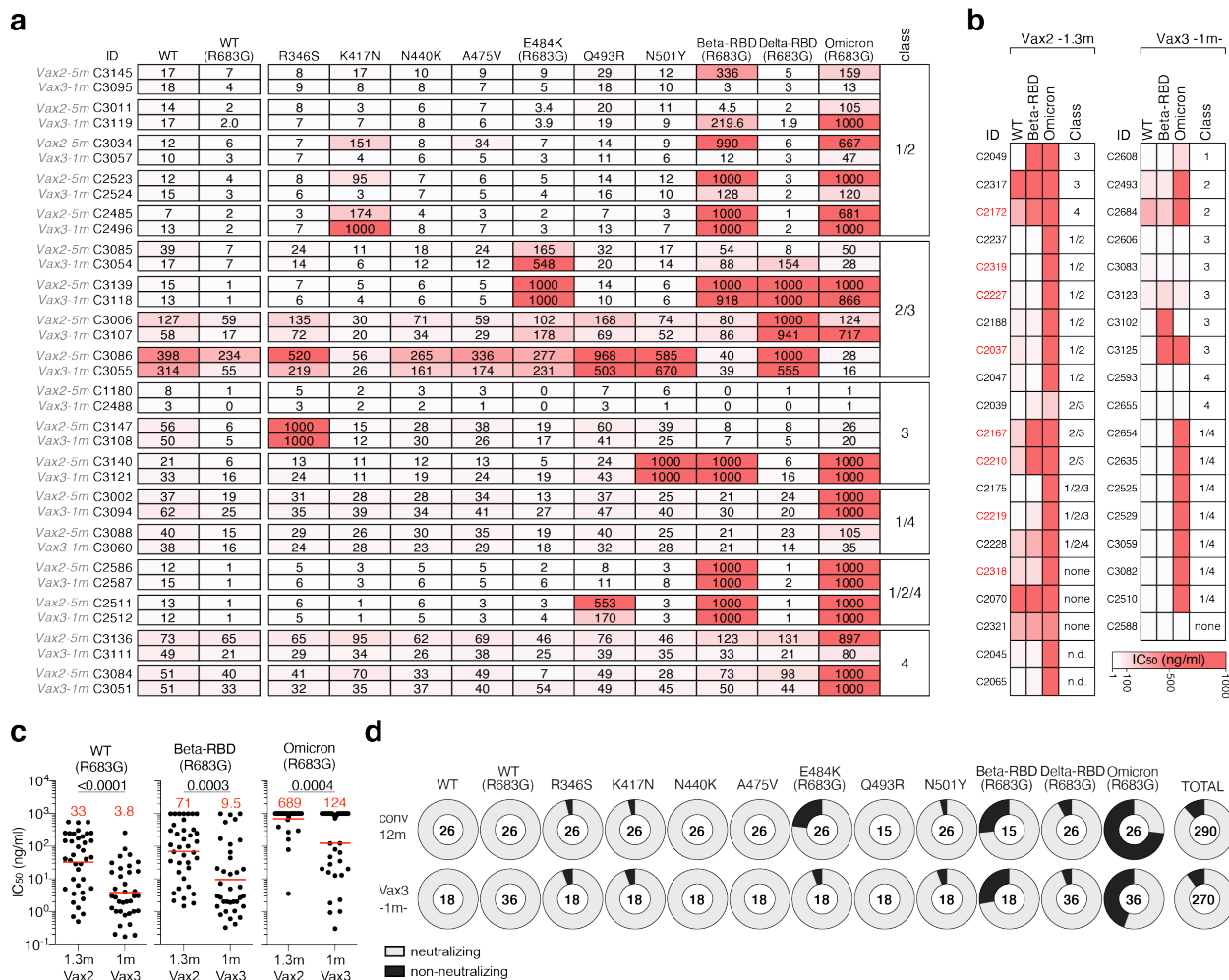
297 **Fig. 3: Anti-SARS-CoV-2 RBD monoclonal antibodies.** **a-b**, Graphs show anti-SARS-CoV-2
 298 neutralizing activity of monoclonal antibodies measured by a SARS-CoV-2 pseudotype virus
 299 neutralization assay using wild-type (Wuhan Hu-1³³) SARS-CoV-2 pseudovirus^{18,34}. IC₅₀ values
 300 for all antibodies (**a**), unique clones, persisting clones, and singlets (**b**). Antibodies were from
 301 vaccinated individuals 1.3 and 5 months after the 2nd vaccine dose (1.3m-Vax2 and 5m-Vax2,
 302 respectively)^{9,10}; 1 month after the 3rd vaccination (1m-Vax3); convalescent individuals 1.3
 303 months¹⁸, or 12 months¹⁷ after infection or vaccinated convalescent individuals 12 months after
 304 infection. Each dot represents one antibody, where 459 total antibodies were tested including the
 305 325 reported herein (Supplementary Table 4), and 134 previously reported¹⁰. Red bars and
 306 numbers indicate geometric mean values. Statistical significance was determined by two-tailed
 307 Kruskal Wallis test with subsequent Dunn's multiple comparisons. All experiments were
 308 performed at least twice.

309



310

311 **Fig. 4: Epitope mapping.** **a**, Diagram represents binding poses of antibodies used in BLI
 312 competition experiments on the RBD epitope. Class 1 antibody (C105, PDB:6XCM) was shown
 313 in orange, class 2 antibody (C144, PDB:7K90) was shown in pink, class 3 antibody (C135
 314 PDB:7K8Z) was shown in gray, and class 4 antibody (C118, PDB:7RKS) was shown in light coral
 315 ^{18,20}. ACE2 epitope of Omicron variant was shown in blue. Omicron mutations were shown in red.
 316 The most conserved residues calculated by the ConSurf Database were shown in yellow (related
 317 to Extended data Fig. 6). **b**, RBD in **a** was enlarged. ACE2 epitope of Omicron variant was
 318 indicated by blue dashed lines, and Omicron mutations were labeled. **c-e**, Results of epitope
 319 mapping performed by competition BLI. Pie charts show the distribution of the antibody classes
 320 among all RBD binding antibodies (**c**), RBD binding antibodies from persisting clones or unique
 321 clones or singlets (**d**), or neutralizing antibodies against Wuhan-Hu-1 (**e**) obtained 1.3- and
 322 5-months after Vax2^{9,10}, and 1 month after 3rd vaccine dose (Vax3). Statistical significance was
 323 determined using a two-tailed Chi-square test.



324

325 **Fig. 5: Breadth.** a-b Heat-maps show IC_{50} s of clonal pairs of antibodies detected 5 months after
 326 the 2nd vaccination (Vax2-5m) persisting 1 month after the 3rd dose (Vax3-1m) (a) and clones and
 327 singlets found 1.3 months after the 2nd (Vax2-1.3m) and uniquely 1 month after the 3rd (Vax3-1m)
 328 vaccine dose (b), against indicated mutant and variant SARS-CoV-2 pseudoviruses listed across
 329 the top. Beta-RBD and Delta-RBD indicate the K417N/E484K/N501Y and L452R/T478K SARS-
 330 CoV-2 spikes, respectively. Heatmap ranging from 0.1-1000 ng/ml in white to red. Antibody
 331 classes in a and b were determined by competition BLI. c, graphs show neutralization activity of
 332 antibodies shown in a and b against WT, Beta-RBD (L452R/T478K) and Omicron, comparing
 333 1.3-month Vax2 and 1-month Vax3 timepoints. Red bars and numbers indicate geometric mean
 334 values. Statistical significance was determined using two-tailed Mann-Whitney test. d, Ring plots
 335 show fraction of neutralizing ($IC_{50}<1000$ ng/ml) and non-neutralizing ($IC_{50}>1000$ ng/ml)
 336 antibodies in light and dark grey, respectively, for indicated SARS-CoV-2 pseudoviruses. Number
 337 in inner circles indicates number of antibodies tested.

338

339 **Methods**

340

341 **Study participants.**

342 Participants were healthy volunteers who had previously received the initial two-dose regimen of
343 either the Moderna (mRNA-1273) or Pfizer-BioNTech (BNT162b2) mRNA vaccines against the
344 wildtype (Wuhan-Hu-1) strain of the severe acute respiratory syndrome coronavirus 2 (SARS-
345 CoV-2). For this study, participants were recruited for serial blood donations at the Rockefeller
346 University Hospital in New York between January 21, 2021, and December 14, 2021. The majority
347 of participants (n=32) were follow-ups from a longitudinal cohort that we previously reported
348 on^{9,10}, while a smaller subgroup of individuals (n=11) was de novo recruited for this study (for
349 details see Supplementary Table 1). Eligible participants (n=43) were healthy adults with no
350 history of infection with SARS-CoV-2 during or prior to the observation period (as determined by
351 clinical history and confirmed through serology testing) who had received two doses of one of the
352 two currently approved SARS-CoV-2 mRNA vaccines, Moderna (mRNA-1273) or Pfizer-
353 BioNTech (BNT162b2), and this also included a subgroup of individuals (n=34) who had received
354 a third vaccine dose. The specifics of each participant's vaccination regimen were at the discretion
355 of the individual and their health care provider consistent with current dosing and interval
356 guidelines and, as such, not influenced by their participation in our study. Exclusion criteria
357 included incomplete vaccination status (defined as less than 2 doses), presence of clinical signs
358 and symptoms suggestive of acute infection with or a positive reverse transcription polymerase
359 chain reaction (RT-PCR) results for SARS-CoV-2 in saliva, or a positive (coronavirus disease
360 2019) COVID-19 serology. Participants presented to the Rockefeller University Hospital for blood
361 sample collection and were asked to provide details of their vaccination regimen, possible side
362 effects, comorbidities and possible COVID-19 history. Clinical data collection and management
363 were carried out using the software iRIS by iMedRIS (v. 11.02). All participants provided written
364 informed consent before participation in the study and the study was conducted in accordance with
365 Good Clinical Practice. The study was performed in compliance with all relevant ethical
366 regulations and the protocol (DRO-1006) for studies with human participants was approved by the
367 Institutional Review Board of the Rockefeller University. For detailed participant characteristics
368 see Supplementary Table 1.

369

370 **Blood samples processing and storage.**

371 Peripheral Blood Mononuclear Cells (PBMCs) obtained from samples collected at Rockefeller
372 University were purified as previously reported by gradient centrifugation and stored in liquid
373 nitrogen in the presence of Fetal Calf Serum (FCS) and Dimethylsulfoxide (DMSO)^{18,19}.
374 Heparinized plasma and serum samples were aliquoted and stored at -20°C or less. Prior to
375 experiments, aliquots of plasma samples were heat-inactivated (56°C for 1 hour) and then stored
376 at 4°C.

377

378 **ELISAs**

379 Enzyme-Linked Immunosorbent Assays (ELISAs)^{35,36} to evaluate antibodies binding to SARS-
380 CoV-2 RBD were performed by coating of high-binding 96-half-well plates (Corning 3690) with
381 50 µl per well of a 1µg/ml protein solution in Phosphate-buffered Saline (PBS) overnight at 4°C.
382 Plates were washed 6 times with washing buffer (1× PBS with 0.05% Tween-20 (Sigma-Aldrich))
383 and incubated with 170 µl per well blocking buffer (1× PBS with 2% BSA and 0.05% Tween-20
384 (Sigma)) for 1 hour at room temperature. Immediately after blocking, monoclonal antibodies or
385 plasma samples were added in PBS and incubated for 1 hour at room temperature. Plasma samples
386 were assayed at a 1:66 starting dilution and 10 additional threefold serial dilutions. Monoclonal
387 antibodies were tested at 10 µg/ml starting concentration and 10 additional fourfold serial dilutions.
388 Plates were washed 6 times with washing buffer and then incubated with anti-human IgG, IgM or
389 IgA secondary antibody conjugated to horseradish peroxidase (HRP) (Jackson Immuno Research
390 109-036-088 109-035-129 and Sigma A0295) in blocking buffer at a 1:5,000 dilution (IgM and
391 IgG) or 1:3,000 dilution (IgA). Plates were developed by addition of the HRP substrate, 3,3',5,5'-
392 Tetramethylbenzidine (TMB) (ThermoFisher) for 10 minutes (plasma samples) or 4 minutes
393 (monoclonal antibodies). The developing reaction was stopped by adding 50 µl of 1 M H₂SO₄ and
394 absorbance was measured at 450 nm with an ELISA microplate reader (FluoStar Omega, BMG
395 Labtech) with Omega and Omega MARS software for analysis. For plasma samples, a positive
396 control (plasma from participant COV72, diluted 66.6-fold and ten additional threefold serial
397 dilutions in PBS) was added to every assay plate for normalization. The average of its signal was
398 used for normalization of all the other values on the same plate with Excel software before
399 calculating the area under the curve using Prism V9.1(GraphPad). Negative controls of pre-
400 pandemic plasma samples from healthy donors were used for validation (for more details please

401 see¹⁸). For monoclonal antibodies, the ELISA half-maximal concentration (EC₅₀) was determined
402 using four-parameter nonlinear regression (GraphPad Prism V9.1). EC₅₀s above 1000 ng/mL were
403 considered non-binders.

404

405 **Proteins**

406 The mammalian expression vector encoding the Receptor Binding-Domain (RBD) of SARS-CoV-
407 2 (GenBank MN985325.1; Spike (S) protein residues 319-539) was previously described³⁷.

408

409 **SARS-CoV-2 pseudotyped reporter virus**

410 A panel of plasmids expressing RBD-mutant SARS-CoV-2 spike proteins in the context of
411 pSARS-CoV-2-S_{Δ19} has been described^{9,10,22,38}. Variant pseudoviruses resembling SARS-CoV-2
412 variants Beta (B.1.351), B.1.526, Delta (B.1.617.2) and Omicron (B.1.1.529) have been described
413 before^{7,10,17} and were generated by introduction of substitutions using synthetic gene fragments
414 (IDT) or overlap extension PCR mediated mutagenesis and Gibson assembly. Specifically, the
415 variant-specific deletions and substitutions introduced were:

416 Beta: D80A, D215G, L242H, R246I, K417N, E484K, N501Y, D614G, A701V

417 DeltaB.1.617.2: T19R, Δ156-158, L452R, T478K, D614G, P681R, D950N

418 Omicron: A67V, Δ69-70, T95I, G142D, Δ143-145, Δ211, L212I, ins214EPE, G339D, S371L,
419 S373P, S375F, K417N, N440K, G446S, S477N, T478K, E484A, Q493K, G496S, Q498R, N501Y,
420 Y505H, T547K, D614G, H655Y, H679K, P681H, N764K, D796Y, N856K, Q954H, N969H,
421 N969K, L981F

422 The E484K, K417N/E484K/N501Y and L452R/T478K substitution, as well as the
423 deletions/substitutions corresponding to variants of concern listed above were incorporated into a
424 spike protein that also includes the R683G substitution, which disrupts the furin cleavage site and
425 increases particle infectivity. Neutralizing activity against mutant pseudoviruses were compared
426 to a wildtype (WT) SARS-CoV-2 spike sequence (NC_045512), carrying R683G where
427 appropriate.

428

429 SARS-CoV-2 pseudotyped particles were generated as previously described^{18,34}. Briefly, 293T
430 (CRL-11268) cells were obtained from ATCC, and the cells were transfected with pNL4-3ΔEnv-

431 nanoluc and pSARS-CoV-2-S_{Δ19}, particles were harvested 48 hours post-transfection, filtered and
432 stored at -80°C.

433

434 **Pseudotyped virus neutralization assay**

435 Fourfold serially diluted pre-pandemic negative control plasma from healthy donors, plasma from
436 individuals who received mRNA vaccines or monoclonal antibodies were incubated with SARS-
437 CoV-2 pseudotyped virus for 1 hour at 37 °C. The mixture was subsequently incubated with
438 293T_{Ace2} cells¹⁸ (for all WT neutralization assays) or HT1080Ace2 c114 (for all mutant panels and
439 variant neutralization assays) cells⁹ for 48 hours after which cells were washed with PBS and lysed
440 with Luciferase Cell Culture Lysis 5× reagent (Promega). Nanoluc Luciferase activity in lysates
441 was measured using the Nano-Glo Luciferase Assay System (Promega) with the Glomax
442 Navigator (Promega). The relative luminescence units were normalized to those derived from cells
443 infected with SARS-CoV-2 pseudotyped virus in the absence of plasma or monoclonal antibodies.
444 The half-maximal neutralization titers for plasma (NT₅₀) or half-maximal and 90% inhibitory
445 concentrations for monoclonal antibodies (IC₅₀ and IC₉₀) were determined using four-parameter
446 nonlinear regression (least squares regression method without weighting; constraints: top=1,
447 bottom=0) (GraphPad Prism).

448

449 **Biotinylation of viral protein for use in flow cytometry**

450 Purified and Avi-tagged SARS-CoV-2 Wuhan-Hu-1 RBD was biotinylated using the Biotin-
451 Protein Ligase-BIRA kit according to manufacturer's instructions (Avidity) as described before¹⁸.
452 Ovalbumin (Sigma, A5503-1G) was biotinylated using the EZ-Link Sulfo-NHS-LC-Biotinylation
453 kit according to the manufacturer's instructions (Thermo Scientific). Biotinylated ovalbumin was
454 conjugated to streptavidin-BV711 for single-cell sorts (BD biosciences, 563262) or to streptavidin-
455 BB515 for phenotyping panel (BD, 564453). RBD was conjugated to streptavidin-PE (BD
456 Biosciences, 554061) and streptavidin-AF647 (Biolegend, 405237)¹⁸.

457

458 **Flow cytometry and single cell sorting**

459 Single-cell sorting by flow cytometry was described previously¹⁸. Briefly, peripheral blood
460 mononuclear cells were enriched for B cells by negative selection using a pan-B-cell isolation kit
461 according to the manufacturer's instructions (Miltenyi Biotec, 130-101-638). The enriched B cells

462 were incubated in Fluorescence-Activated Cell-sorting (FACS) buffer (1× PBS, 2% FCS, 1 mM
463 ethylenediaminetetraacetic acid (EDTA)) with the following anti-human antibodies (all at 1:200
464 dilution): anti-CD20-PECy7 (BD Biosciences, 335793), anti-CD3-APC-eFluor 780 (Invitrogen,
465 47-0037-41), anti-CD8-APC-eFluor 780 (Invitrogen, 47-0086-42), anti-CD16-APC-eFluor 780
466 (Invitrogen, 47-0168-41), anti-CD14-APC-eFluor 780 (Invitrogen, 47-0149-42), as well as
467 Zombie NIR (BioLegend, 423105) and fluorophore-labeled RBD and ovalbumin (Ova) for 30 min
468 on ice. Single CD3-CD8-CD14-CD16-CD20+Ova-RBD-PE+RBD-AF647+ B cells were sorted
469 into individual wells of 96-well plates containing 4 µl of lysis buffer (0.5× PBS, 10 mM
470 Dithiothreitol (DTT), 3,000 units/ml RNasin Ribonuclease Inhibitors (Promega, N2615) per well
471 using a FACS Aria III and FACSDiva software (Becton Dickinson) for acquisition and FlowJo for
472 analysis. The sorted cells were frozen on dry ice, and then stored at -80 °C or immediately used
473 for subsequent RNA reverse transcription. For B cell phenotype analysis, in addition to above
474 antibodies, B cells were also stained with following anti-human antibodies (all at 1:200 dilution):
475 anti-IgD-BV650 (BD, 740594), anti-CD27-BV786 (BD biosciences, 563327), anti-CD19-BV605
476 (Biolegend, 302244), anti-CD71- PerCP-Cy5.5 (Biolegend, 334114), anti- IgG-PECF594 (BD,
477 562538), anti-IgM-AF700 (Biolegend, 314538), anti-IgA-Viogreen (Miltenyi Biotec, 130-113-
478 481).

479

480 **Antibody sequencing, cloning and expression**

481 Antibodies were identified and sequenced as described previously^{18,39}. In brief, RNA from single
482 cells was reverse-transcribed (SuperScript III Reverse Transcriptase, Invitrogen, 18080-044) and
483 the cDNA was stored at -20 °C or used for subsequent amplification of the variable IGH, IGL and
484 IGK genes by nested PCR and Sanger sequencing. Sequence analysis was performed using
485 MacVector. Amplicons from the first PCR reaction were used as templates for sequence- and
486 ligation-independent cloning into antibody expression vectors. Recombinant monoclonal
487 antibodies were produced and purified as previously described¹⁸.

488

489 **Biolayer interferometry**

490 Biolayer interferometry assays were performed as previously described¹⁸. Briefly, we used the
491 Octet Red instrument (ForteBio) at 30 °C with shaking at 1,000 r.p.m. Epitope binding assays
492 were performed with protein A biosensor (ForteBio 18-5010), following the manufacturer's

493 protocol “classical sandwich assay” as follows: (1) Sensor check: sensors immersed 30 sec in
494 buffer alone (buffer ForteBio 18-1105), (2) Capture 1st Ab: sensors immersed 10 min with Ab1 at
495 10 $\mu\text{g}/\text{mL}$, (3) Baseline: sensors immersed 30 sec in buffer alone, (4) Blocking: sensors immersed
496 5 min with IgG isotype control at 10 $\mu\text{g}/\text{mL}$. (5) Baseline: sensors immersed 30 sec in buffer alone,
497 (6) Antigen association: sensors immersed 5 min with RBD at 10 $\mu\text{g}/\text{mL}$. (7) Baseline: sensors
498 immersed 30 sec in buffer alone. (8) Association Ab2: sensors immersed 5 min with Ab2 at 10
499 $\mu\text{g}/\text{mL}$. Curve fitting was performed using the Fortebio Octet Data analysis software (ForteBio).

500

501 **Computational analyses of antibody sequences**

502 Antibody sequences were trimmed based on quality and annotated using Igblastn v.1.14. with
503 IMGT domain delineation system. Annotation was performed systematically using Change-O
504 toolkit v.0.4.540⁴⁰. Heavy and light chains derived from the same cell were paired, and clonotypes
505 were assigned based on their V and J genes using in-house R and Perl scripts. All scripts and the
506 data used to process antibody sequences are publicly available on GitHub
507 (https://github.com/stratust/igpipeline/tree/igpipeline2_timepoint_v2).

508 The frequency distributions of human V genes in anti-SARS-CoV-2 antibodies from this study
509 was compared to 131,284,220 IgH and IGL sequences generated by⁴¹ and downloaded from cAb-
510 Rep⁴², a database of human shared BCR clonotypes available at [https://cab-](https://cab-rep.c2b2.columbia.edu/)
511 [rep.c2b2.columbia.edu/](https://cab-rep.c2b2.columbia.edu/). Based on the 150 distinct V genes that make up the 1650 analyzed
512 sequences from Ig repertoire of the 5 participants present in this study, we selected the IgH and
513 IGL sequences from the database that are partially coded by the same V genes and counted them
514 according to the constant region. The frequencies shown in Extended Data Fig. 3 are relative to
515 the source and isotype analyzed. We used the two-sided binomial test to check whether the number
516 of sequences belonging to a specific IGHV or IGLV gene in the repertoire is different according
517 to the frequency of the same IgV gene in the database. Adjusted p-values were calculated using
518 the false discovery rate (FDR) correction. Significant differences are denoted with stars.

519

520 Nucleotide somatic hypermutation and Complementarity-Determining Region (CDR3) length
521 were determined using in-house R and Perl scripts. For somatic hypermutations, *IGHV* and *IGLV*
522 nucleotide sequences were aligned against their closest germlines using Igblastn and the number
523 of differences were considered nucleotide mutations. The average number of mutations for V

524 genes was calculated by dividing the sum of all nucleotide mutations across all participants by the
525 number of sequences used for the analysis.

526

527 **Data presentation**

528 Figures arranged in Adobe Illustrator 2022.

529

530 **Data availability statement:** Data are provided in Supplementary Tables 1-4. The raw sequencing
531 data and computer scripts associated with Figure 2 have been deposited at Github
532 (https://github.com/stratust/igpipeline/tree/igpipeline2_timepoint_v2). This study also uses data
533 from “A Public Database of Memory and Naive B-Cell Receptor Sequences”
534 (<https://doi.org/10.5061/dryad.35ks2>), PDB (6VYB and 6NB6), cAb-Rep ([https://cab-](https://cab-rep.c2b2.columbia.edu/)
535 [rep.c2b2.columbia.edu/](https://cab-rep.c2b2.columbia.edu/)), Sequence Read Archive (accession SRP010970), and from “High
536 frequency of shared clonotypes in human B cell receptor repertoires”
537 (<https://doi.org/10.1038/s41586-019-0934-8>).

538

539 **Code availability statement:** Computer code to process the antibody sequences is available at
540 GitHub (https://github.com/stratust/igpipeline/tree/igpipeline2_timepoint_v2).

541

542 **Reference**

- 543 1 Chaguza, C. *et al.* Rapid emergence of SARS-CoV-2 Omicron variant is associated with an
544 infection advantage over Delta in vaccinated persons. *medRxiv*,
545 2022.2001.2022.22269660, doi:10.1101/2022.01.22.22269660 (2022).
- 546 2 Kuhlmann, C. *et al.* Breakthrough infections with SARS-CoV-2 omicron despite mRNA
547 vaccine booster dose. *Lancet*, doi:10.1016/S0140-6736(22)00090-3 (2022).
- 548 3 Nemet, I. *et al.* Third BNT162b2 Vaccination Neutralization of SARS-CoV-2 Omicron
549 Infection. *N Engl J Med* **386**, 492-494, doi:10.1056/NEJMc2119358 (2022).
- 550 4 Rossler, A., Riepler, L., Bante, D., von Laer, D. & Kimpel, J. SARS-CoV-2 Omicron Variant
551 Neutralization in Serum from Vaccinated and Convalescent Persons. *N Engl J Med*,
552 doi:10.1056/NEJMc2119236 (2022).
- 553 5 Liu, L. *et al.* Striking Antibody Evasion Manifested by the Omicron Variant of SARS-CoV-2.
554 *Nature*, doi:10.1038/s41586-021-04388-0 (2021).
- 555 6 Carreno, J. M. *et al.* Activity of convalescent and vaccine serum against SARS-CoV-2
556 Omicron. *Nature*, doi:10.1038/s41586-022-04399-5 (2021).
- 557 7 Schmidt, F. *et al.* Plasma Neutralization of the SARS-CoV-2 Omicron Variant. *N Engl J Med*,
558 doi:10.1056/NEJMc2119641 (2021).

- 559 8 Danza, P. *et al.* SARS-CoV-2 Infection and Hospitalization Among Adults Aged ≥ 18 Years,
560 by Vaccination Status, Before and During SARS-CoV-2 B.1.1.529 (Omicron) Variant
561 Predominance - Los Angeles County, California, November 7, 2021-January 8, 2022.
562 *MMWR Morb Mortal Wkly Rep* **71**, 177-181, doi:10.15585/mmwr.mm7105e1 (2022).
- 563 9 Wang, Z. *et al.* mRNA vaccine-elicited antibodies to SARS-CoV-2 and circulating variants.
564 *Nature* **592**, 616-622, doi:10.1038/s41586-021-03324-6 (2021).
- 565 10 Cho, A. *et al.* Anti-SARS-CoV-2 receptor-binding domain antibody evolution after mRNA
566 vaccination. *Nature* **600**, 517-522, doi:10.1038/s41586-021-04060-7 (2021).
- 567 11 Gruell, H. *et al.* mRNA booster immunization elicits potent neutralizing serum activity
568 against the SARS-CoV-2 Omicron variant. *Nat Med*, doi:10.1038/s41591-021-01676-0
569 (2022).
- 570 12 Wang, K. *et al.* Memory B cell repertoire from triple vaccinees against diverse SARS-CoV-
571 2 variants. *Nature*, doi:10.1038/s41586-022-04466-x (2022).
- 572 13 Pajon, R. *et al.* SARS-CoV-2 Omicron Variant Neutralization after mRNA-1273 Booster
573 Vaccination. *N Engl J Med*, doi:10.1056/NEJMc2119912 (2022).
- 574 14 Cromer, D. *et al.* Neutralising antibody titres as predictors of protection against SARS-
575 CoV-2 variants and the impact of boosting: a meta-analysis. *Lancet Microbe* **3**, e52-e61,
576 doi:10.1016/S2666-5247(21)00267-6 (2022).
- 577 15 Khoury, D. S. *et al.* Neutralizing antibody levels are highly predictive of immune protection
578 from symptomatic SARS-CoV-2 infection. *Nat Med* **27**, 1205-1211, doi:10.1038/s41591-
579 021-01377-8 (2021).
- 580 16 Victora, G. D. & Nussenzweig, M. C. Germinal Centers. *Annu Rev Immunol*,
581 doi:10.1146/annurev-immunol-120419-022408 (2022).
- 582 17 Wang, Z. *et al.* Naturally enhanced neutralizing breadth against SARS-CoV-2 one year after
583 infection. *Nature*, doi:10.1038/s41586-021-03696-9 (2021).
- 584 18 Robbiani, D. F. *et al.* Convergent antibody responses to SARS-CoV-2 in convalescent
585 individuals. *Nature* **584**, 437-442, doi:10.1038/s41586-020-2456-9 (2020).
- 586 19 Gaebler, C. *et al.* Evolution of antibody immunity to SARS-CoV-2. *Nature* **591**, 639-644,
587 doi:10.1038/s41586-021-03207-w (2021).
- 588 20 Barnes, C. O. *et al.* SARS-CoV-2 neutralizing antibody structures inform therapeutic
589 strategies. *Nature* **588**, 682-687, doi:10.1038/s41586-020-2852-1 (2020).
- 590 21 Yuan, M. *et al.* Structural basis of a shared antibody response to SARS-CoV-2. *Science* **369**,
591 1119-1123, doi:10.1126/science.abd2321 (2020).
- 592 22 Muecksch, F. *et al.* Affinity maturation of SARS-CoV-2 neutralizing antibodies confers
593 potency, breadth, and resilience to viral escape mutations. *Immunity* **54**, 1853-1868
594 e1857, doi:10.1016/j.immuni.2021.07.008 (2021).
- 595 23 Viant, C. *et al.* Antibody Affinity Shapes the Choice between Memory and Germinal Center
596 B Cell Fates. *Cell* **183**, 1298-1311 e1211, doi:10.1016/j.cell.2020.09.063 (2020).
- 597 24 Viant, C. *et al.* Germinal center-dependent and -independent memory B cells produced
598 throughout the immune response. *J Exp Med* **218**, doi:10.1084/jem.20202489 (2021).
- 599 25 Zhang, Y. *et al.* Germinal center B cells govern their own fate via antibody feedback. *J Exp*
600 *Med* **210**, 457-464, doi:10.1084/jem.20120150 (2013).
- 601 26 Gupta, A. *et al.* Early Treatment for Covid-19 with SARS-CoV-2 Neutralizing Antibody
602 Sotrovimab. *N Engl J Med* **385**, 1941-1950, doi:10.1056/NEJMoa2107934 (2021).

- 603 27 Taylor, P. C. *et al.* Neutralizing monoclonal antibodies for treatment of COVID-19. *Nat Rev*
604 *Immunol* **21**, 382-393, doi:10.1038/s41577-021-00542-x (2021).
- 605 28 Li, D., Sempowski, G. D., Saunders, K. O., Acharya, P. & Haynes, B. F. SARS-CoV-2
606 Neutralizing Antibodies for COVID-19 Prevention and Treatment. *Annu Rev Med* **73**, 1-16,
607 doi:10.1146/annurev-med-042420-113838 (2022).
- 608 29 Weinreich, D. M. *et al.* REGN-COV2, a Neutralizing Antibody Cocktail, in Outpatients with
609 Covid-19. *N Engl J Med* **384**, 238-251, doi:10.1056/NEJMoa2035002 (2021).
- 610 30 O'Brien, M. P., Hou, P. & Weinreich, D. M. Subcutaneous REGEN-COV Antibody
611 Combination to Prevent Covid-19. Reply. *N Engl J Med* **385**, e70,
612 doi:10.1056/NEJMc2113862 (2021).
- 613 31 Wrammert, J. *et al.* Rapid cloning of high-affinity human monoclonal antibodies against
614 influenza virus. *Nature* **453**, 667-671, doi:10.1038/nature06890 (2008).
- 615 32 Gottlieb, R. L. *et al.* Effect of Bamlanivimab as Monotherapy or in Combination With
616 Etesevimab on Viral Load in Patients With Mild to Moderate COVID-19: A Randomized
617 Clinical Trial. *JAMA* **325**, 632-644, doi:10.1001/jama.2021.0202 (2021).
- 618 33 Wu, F. *et al.* A new coronavirus associated with human respiratory disease in China.
619 *Nature* **579**, 265-269, doi:10.1038/s41586-020-2008-3 (2020).
- 620 34 Schmidt, F. *et al.* Measuring SARS-CoV-2 neutralizing antibody activity using pseudotyped
621 and chimeric viruses. *J Exp Med* **217**, doi:10.1084/jem.20201181 (2020).
- 622 35 Amanat, F. *et al.* A serological assay to detect SARS-CoV-2 seroconversion in humans. *Nat*
623 *Med* **26**, 1033-1036, doi:10.1038/s41591-020-0913-5 (2020).
- 624 36 Grifoni, A. *et al.* Targets of T Cell Responses to SARS-CoV-2 Coronavirus in Humans with
625 COVID-19 Disease and Unexposed Individuals. *Cell* **181**, 1489-1501 e1415,
626 doi:10.1016/j.cell.2020.05.015 (2020).
- 627 37 Barnes, C. O. *et al.* Structures of Human Antibodies Bound to SARS-CoV-2 Spike Reveal
628 Common Epitopes and Recurrent Features of Antibodies. *Cell* **182**, 828-842 e816,
629 doi:10.1016/j.cell.2020.06.025 (2020).
- 630 38 Weisblum, Y. *et al.* Escape from neutralizing antibodies by SARS-CoV-2 spike protein
631 variants. *Elife* **9**, doi:10.7554/eLife.61312 (2020).
- 632 39 Wang, Z. *et al.* Enhanced SARS-CoV-2 neutralization by dimeric IgA. *Sci Transl Med* **13**,
633 doi:10.1126/scitranslmed.abf1555 (2021).
- 634 40 Gupta, N. T. *et al.* Change-O: a toolkit for analyzing large-scale B cell immunoglobulin
635 repertoire sequencing data. *Bioinformatics* **31**, 3356-3358,
636 doi:10.1093/bioinformatics/btv359 (2015).
- 637 41 Soto, C. *et al.* High frequency of shared clonotypes in human B cell receptor repertoires.
638 *Nature* **566**, 398-402, doi:10.1038/s41586-019-0934-8 (2019).
- 639 42 Guo, Y., Chen, K., Kwong, P. D., Shapiro, L. & Sheng, Z. cAb-Rep: A Database of Curated
640 Antibody Repertoires for Exploring Antibody Diversity and Predicting Antibody
641 Prevalence. *Front Immunol* **10**, 2365, doi:10.3389/fimmu.2019.02365 (2019).
- 642 43 Sievers, F. *et al.* Fast, scalable generation of high-quality protein multiple sequence
643 alignments using Clustal Omega. *Mol Syst Biol* **7**, 539, doi:10.1038/msb.2011.75 (2011).
- 644 44 Landau, M. *et al.* ConSurf 2005: the projection of evolutionary conservation scores of
645 residues on protein structures. *Nucleic Acids Res* **33**, W299-302, doi:10.1093/nar/gki370
646 (2005).

647 **Acknowledgements:** We thank all study participants who devoted time to our research, The
648 Rockefeller University Hospital nursing staff and Clinical Research Support Office. We thank all
649 members of the M.C.N. laboratory for helpful discussions, Maša Jankovic for laboratory support
650 and Kristie Gordon for technical assistance with cell-sorting experiments. This work was
651 supported by NIH grant P01-AI138398-S1 (M.C.N.) and 2U19AI111825 (M.C.N.). R37-AI64003
652 to P.D.B.; R01AI78788 to T.H.. F.M. was supported by the Bulgari Women and Science
653 Fellowship for COVID-19 Research. C.G. was supported by the Robert S. Wennett Post-Doctoral
654 Fellowship, in part by the National Center for Advancing Translational Sciences (National
655 Institutes of Health Clinical and Translational Science Award program, grant UL1 TR001866),
656 and by the Shapiro-Silverberg Fund for the Advancement of Translational Research. P.D.B. and
657 M.C.N. are Howard Hughes Medical Institute Investigators. This article is subject to HHMI's
658 Open Access to Publications policy. HHMI lab heads have previously granted a nonexclusive CC
659 BY 4.0 license to the public and a sublicensable license to HHMI in their research articles. Pursuant
660 to those licenses, the author-accepted manuscript of this article can be made freely available under
661 a CC BY 4.0 license immediately upon publication.

662

663 **Author information:** F.M. Z.W. and A.C. contributed equally to this work.

664

665 **Author Contributions:** F.M., Z.W., A.C., T.H., P.D.B., and M.C.N. conceived, designed, and
666 analyzed the experiments. M. Caskey and C.G. designed clinical protocols. F.M. Z.W., A.C.,
667 T.B.T, J.D., E.B., S.Z., R.R., D.S.-B., K.Y., and F.S. carried out experiments. B.J. and A.G.,
668 produced antibodies. M.T., K.G.M., I.S., M.D., C.G. and M.C. recruited participants, executed
669 clinical protocols, and processed samples. T.Y.O. and V.R. performed bioinformatic analysis.
670 F.M., Z.W., A.C., T.H., P.D.B., and M.C.N. wrote the manuscript with input from all co-authors.

671

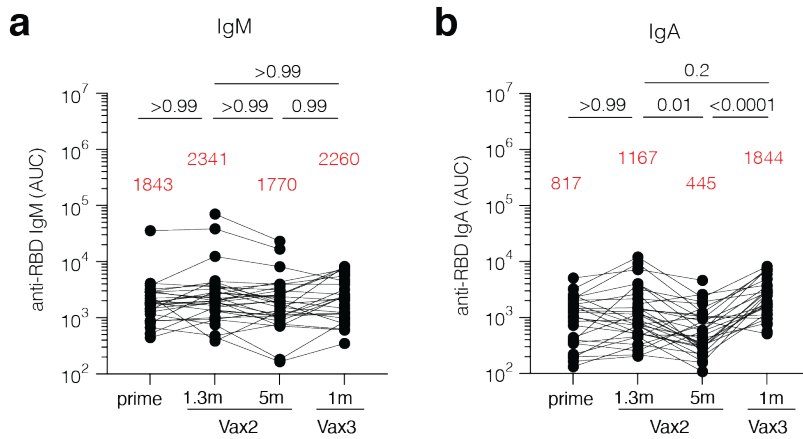
672 **Corresponding authors:** Correspondence should be addressed to Theodora Hatzioannou, Paul
673 D. Bieniasz, or Michel C. Nussenzweig.

674

675 **Declaration of interests:** The Rockefeller University has filed a provisional patent application in
676 connection with this work on which M.C.N. is an inventor (US patent 63/021,387). P.D.B. has
677 received remuneration from Pfizer for consulting services relating to SARS-CoV-2 vaccines.

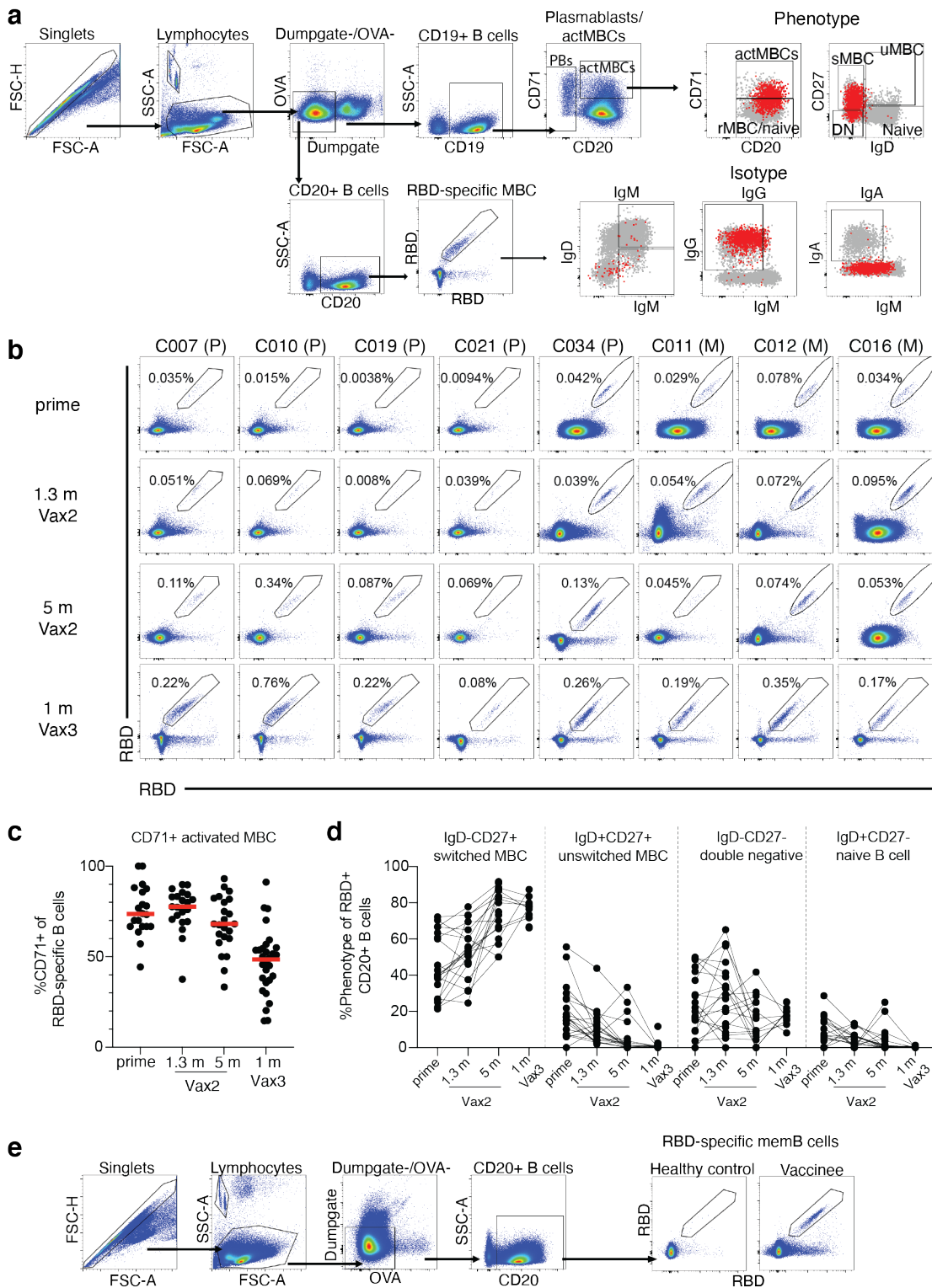
678 **Extended data Figures**

679



680

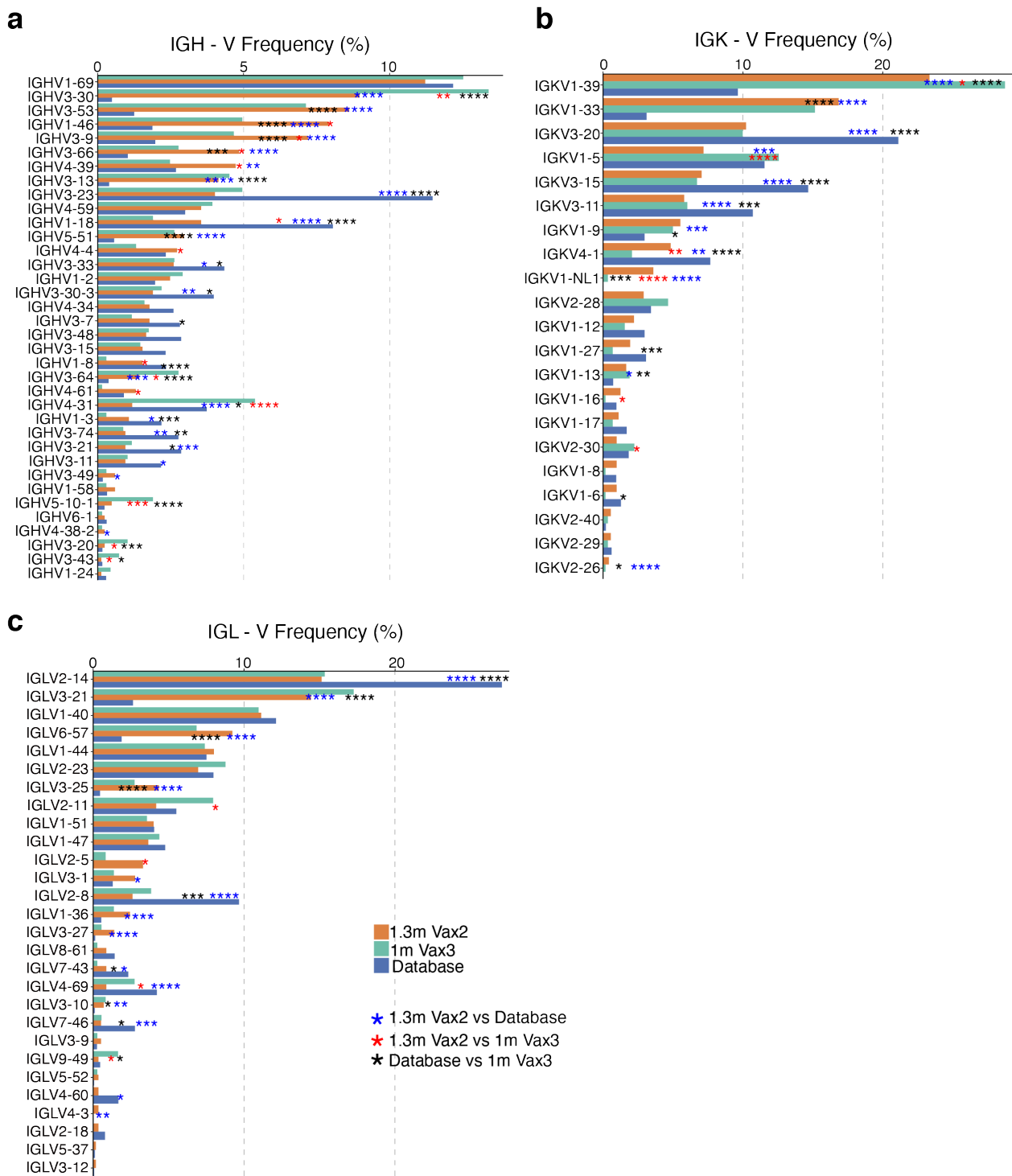
681 **Extended Data Fig. 1: Plasma ELISA.** Graph shows area under the curve (AUC) for plasma **a**,
682 IgM and **b**, IgA antibody binding to SARS-CoV-2 RBD after prime¹⁰, 1.3 months (m) and 5
683 months (m) after the 2nd vaccine dose (Vax2)^{9,10}, and 1 month after the 3rd (Vax3) for n=43
684 samples. Lines connect longitudinal samples. Red bars and value represent geometric mean values.
685 Statistical significance was determined by two-tailed Kruskal-Wallis test with subsequent Dunn's
686 multiple comparisons.



687

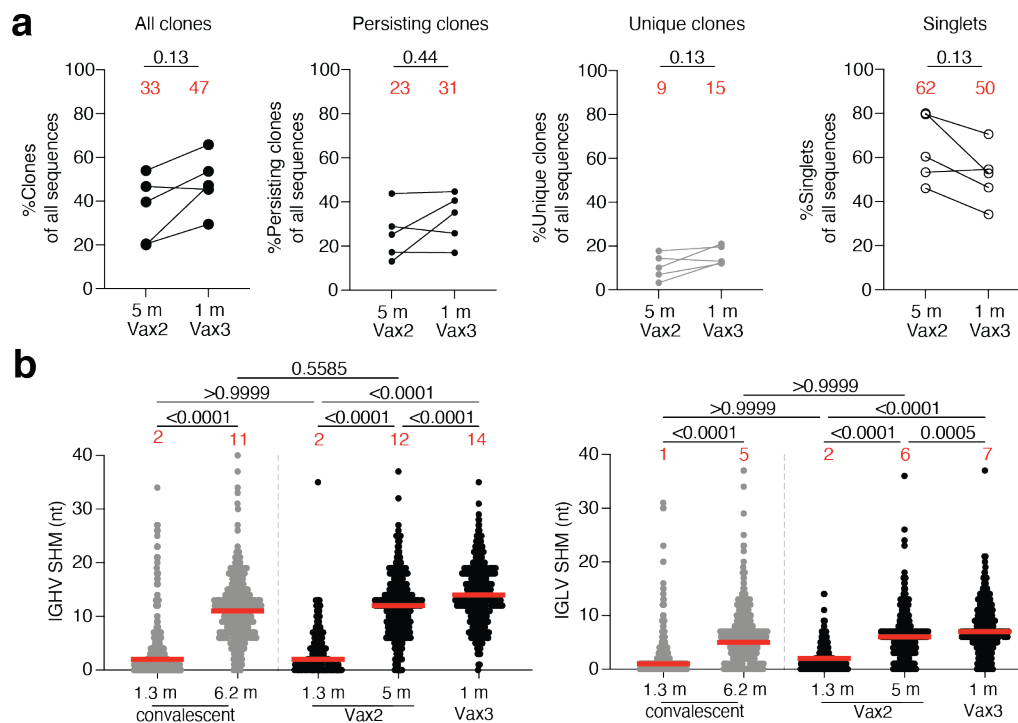
688 **Extended Data Fig. 2: Flow Cytometry.** **a**, Gating strategy for phenotyping. Gating was on
 689 lymphocytes singlets that were CD19⁺ or CD20⁺ and CD3-CD8-CD16-Ova-. Anti-IgG, IgM, IgA,
 690 IgD, CD71 and CD27 antibodies were used for B cell phenotype analysis. Antigen-specific cells
 691 were detected based on binding to Wuhan-Hu-1 RBD-PE⁺ and RBD-AF647⁺. **b**, Representative

692 flow cytometry plots of RBD-binding memory B cells in 8 individuals after prime¹⁰, 1.3- and 5-
693 months post-Vax2^{9,10}, and 1 month after Vax3. Time point of sample collection indicated to the
694 left. Pfizer vaccinees indicated by (P) and Moderna by (M) across the top. **c**, Graph showing
695 frequency of RBD-specific MBCs expressing activation marker CD71 over time after vaccination
696 for n=36 samples. Red bar indicated median value. **d**, Graph showing the phenotype of RBD-
697 specific B cells over time, determined to be either switched MBCs (IgD-CD27+), unswitched
698 MBCs (IgD+CD27+), double negative MBCs (IgD-CD27-) or naïve B cells (IgD+CD27+), for
699 n=18 samples. Lines connect longitudinal samples. **f**, Gating strategy for single-cell sorting for
700 CD20+ memory B cells for RBD-PE and RBD-AF647.



701

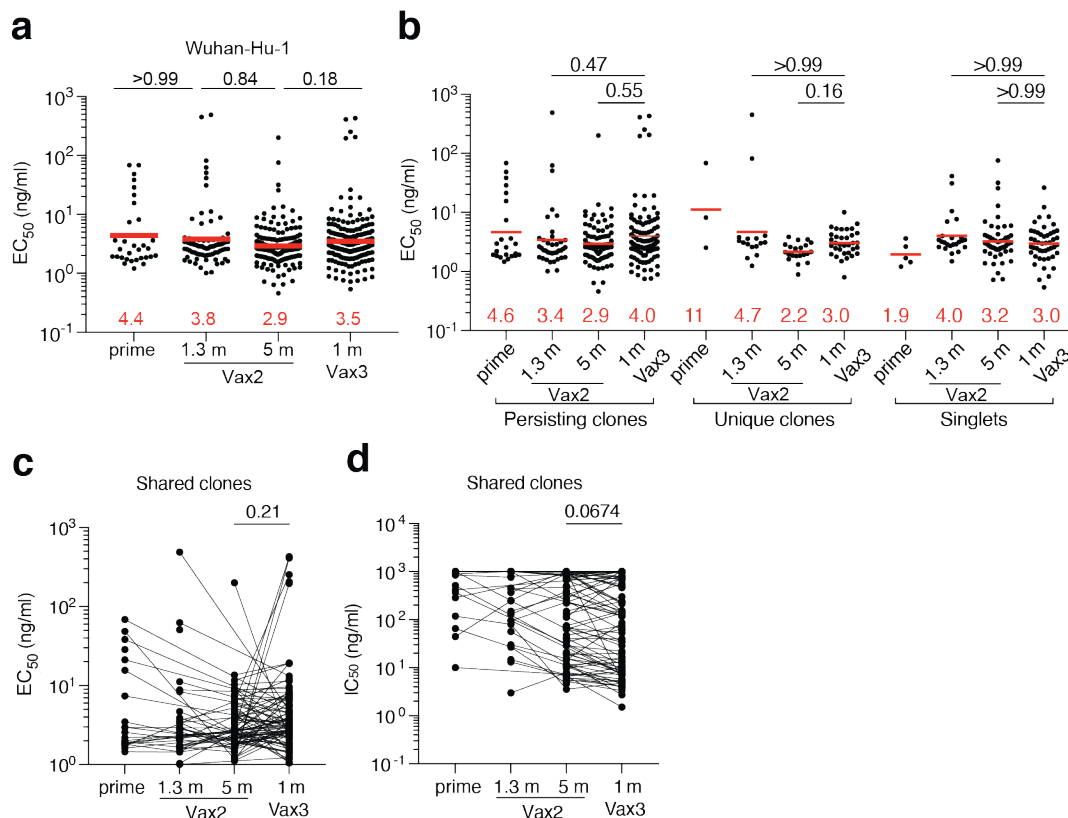
702 **Extended Data Fig. 3: Frequency distribution of human V genes.** a-c Comparison of the
 703 frequency distribution of human V genes for heavy chain and light chains of anti-RBD antibodies
 704 from this study and from a database of shared clonotypes of human B cell receptor generated by
 705 Cinque Soto et al⁴¹. Graph shows relative abundance of human IGHV (a), IGKV (b) and IGLV
 706 (c) genes Sequence Read Archive accession SRP010970 (blue), 1.3m-Vax 2 antibodies (orange),
 707 and 1m-Vax3 antibodies (green).



708

709 **Extended Data Fig. 4: Clonality and somatic hypermutation of anti-SARS-CoV-2 RBD**
 710 **antibody clones after third vaccination booster.** **a**, Graphs show relative fraction of clones,
 711 persisting clones, unique clones and singlets among all antibody sequences in n=5 individuals 5m
 712 after the 2nd and 1 month after the 3rd dose. **b**, Number of nucleotide somatic hypermutations
 713 (SHM) in the *IGHV* (left panel) and *IGLV* (right panel) in the antibodies illustrated in **Fig. 2c** for
 714 vaccinees after 1.3- and 5- months post-Vax2^{9,10} and 1 month after Vax3, compared to the number
 715 of mutations obtained after 1.3¹⁸ or 6.2¹⁹ months after infection (grey).

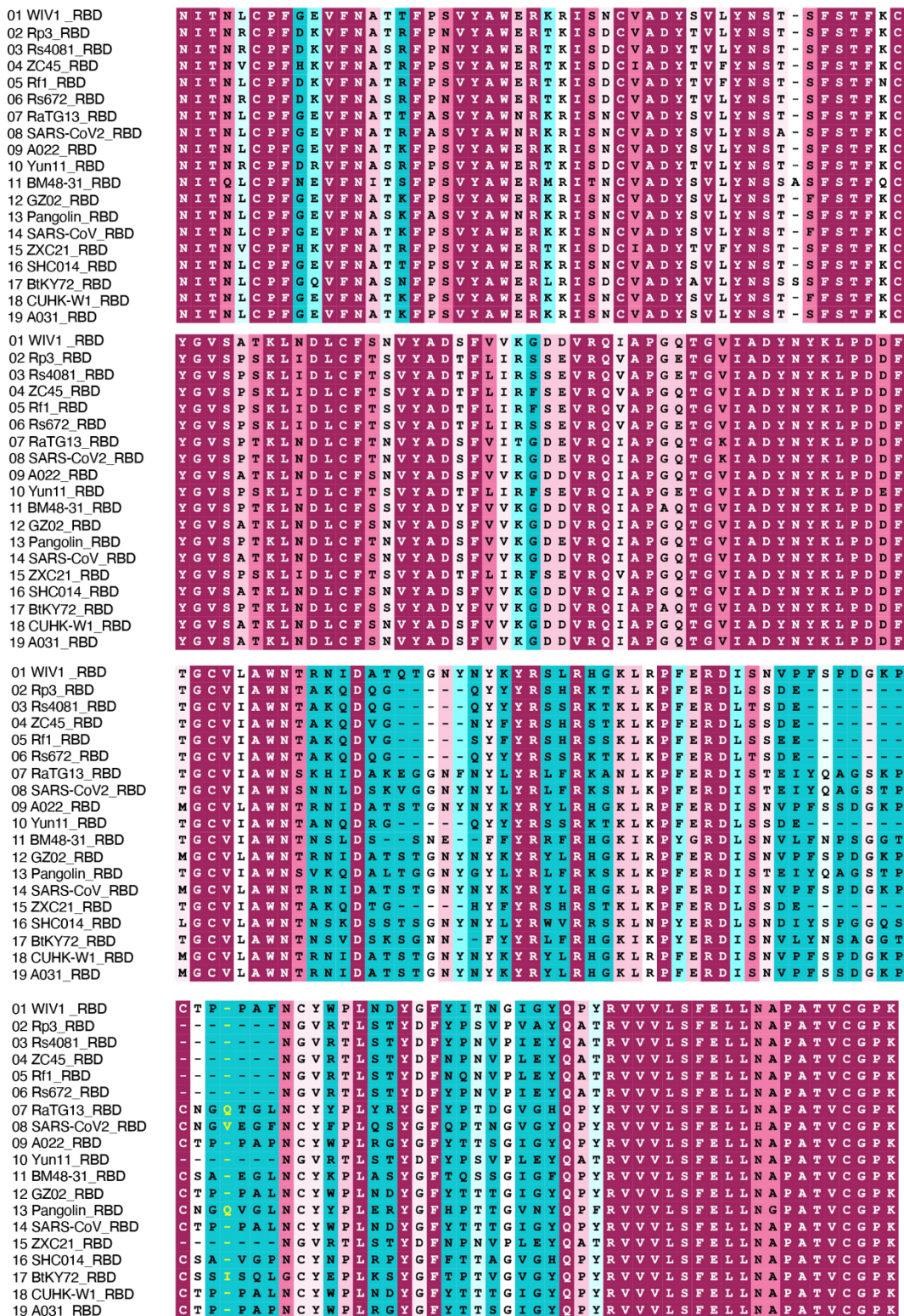
716
717



718

719 **Extended Data Fig. 5: Anti-SARS-CoV-2 RBD monoclonal antibodies.** **a**, Graphs show half-
720 maximal concentration (EC₅₀) of n=459 monoclonal antibodies measured by ELISA against
721 Wuhan-Hu-1 RBD after prime¹⁰, 1.3- and 5-months post-Vax2^{9,10}, and 1 month after Vax3. **b**,
722 Graph showing EC₅₀ of monoclonal antibodies as categorized as either persisting clones detected
723 at multiple time points, unique clones where sequences were clonally expanded but detected at a
724 single time point, or singlets were mAbs were derived from sequences detected once at a single
725 time point. Graph showing **c**, EC₅₀ of monoclonal antibodies or **d**, IC₅₀ neutralizing activity from
726 antibodies derived from shared clones only. Lines connect the related clones at the indicated time
727 point. Red bars and numbers in **a**, and **b**, indicate geometric mean values. Statistical significance
728 was determined by two-tailed Kruskal Wallis test with subsequent Dunn's multiple comparisons.
729 All experiments were performed at least twice.

ConSurf Color-Coded Multiple Sequence Alignment



1 2 3 4 5 6 7 8 9
Variable Average Conserved

731 **Extended Data Fig. 6. Multiple sequence alignment of RBDs.** Sequences used for the alignment
732 are the RBDs of WIV1(GenBank: KF367457.1), Rp3(UniprotKB:Q3I5J5), Rs4081(GenBank:
733 KY417143.1), ZC45 (GenBank: AVP78031.1), Rf1(GenBank: DQ412042.1), Rs672(GenBank:
734 ACU31032.1), RaTG13(GenBank: QHR63300.2), SARS-CoV2 (GenBank: MN985325.1),
735 A022(GenBank: AAV91631.1), Yun11 (GenBank: JX993988.1), BM48-31(NCBI Reference
736 Sequence: NC_014470.1), GZ02(GenBank: AAS00003.1), Pangolin(GenBank: QIA48632.1),
737 SARS-CoV(UniProtKB:P59594), ZXC21(GenBank: AVP78042.1), SHC014(GenBank:
738 KC881005.1), BtKY72(GenBank: KY352407.1), CUHK-W1(GenBank: AAP13567.1), and
739 A031(GenBank: AAV97988.1). Multiple sequence alignment of RBDs was processed by Clustal
740 Omega⁴³. Sequence conservation was calculated by the ConSurf Database⁴⁴.

741

742

743 **Supplementary Information**

744

745 **Supplementary Table 1:** Individual participant characteristics.

746 **Supplementary Table 2:** Sequences of anti-SARS-CoV-2 RBD IgG antibodies.

747 **Supplementary Table 3:** Sequences, half-maximal effective concentrations (EC₅₀s) and
748 inhibitory concentrations (IC₅₀s) of cloned monoclonal antibodies.

749

750 **Supplementary Table 4:** Binding and Neutralization activity of persisting clones

751